Accepted Manuscript

Title: Polyaniline based hybrid bionanocomposites with enhanced visible light photocatalytic activity and antifungal activity

Authors: Nafees Ahmad, Saima Sultana, Greesh Kumar, Mohammad Zuhaib, Suhail Sabir, Mohammad Zain Khan

PII: S2213-3437(18)30727-9
DOI: https://doi.org/10.1016/j.jece.2018.11.048
Reference: JECE 2804

To appear in:

Received date: 5 October 2018
Revised date: 16 November 2018
Accepted date: 22 November 2018

Please cite this article as: Ahmad N, Sultana S, Kumar G, Zuhaib M, Sabir S, Khan MZ, Polyaniline based hybrid bionanocomposites with enhanced visible light photocatalytic activity and antifungal activity, *Journal of Environmental Chemical Engineering* (2018), https://doi.org/10.1016/j.jece.2018.11.048

This is a PDF file of an unedited manuscript that has been accepted for publication. As a service to our customers we are providing this early version of the manuscript. The manuscript will undergo copyediting, typesetting, and review of the resulting proof before it is published in its final form. Please note that during the production process errors may be discovered which could affect the content, and all legal disclaimers that apply to the journal pertain.

ACCEPTED MANUSCRIPT

Polyaniline based hybrid bionanocomposites with enhanced visible light photocatalytic activity and antifungal activity

Nafees Ahmad[1], Saima Sultana[1], Greesh Kumar[1], Mohammad Zuhaib[2], Suhail Sabir[1], Mohammad Zain Khan[1*]

[1]Environmental Research Laboratory, Department of Chemistry, Faculty of Sciences, Aligarh Muslim University, Aligarh 202 002, Uttar Pradesh, India
[2]Department of Plant Protection, Faculty of Agricultural Sciences, Aligarh Muslim University, Aligarh 202 002, Uttar Pradesh, India

GRAPHICAL ABSTRACT

ACCEPTED MANUSCRIPT

ACCEPTED MANUSCRIPT

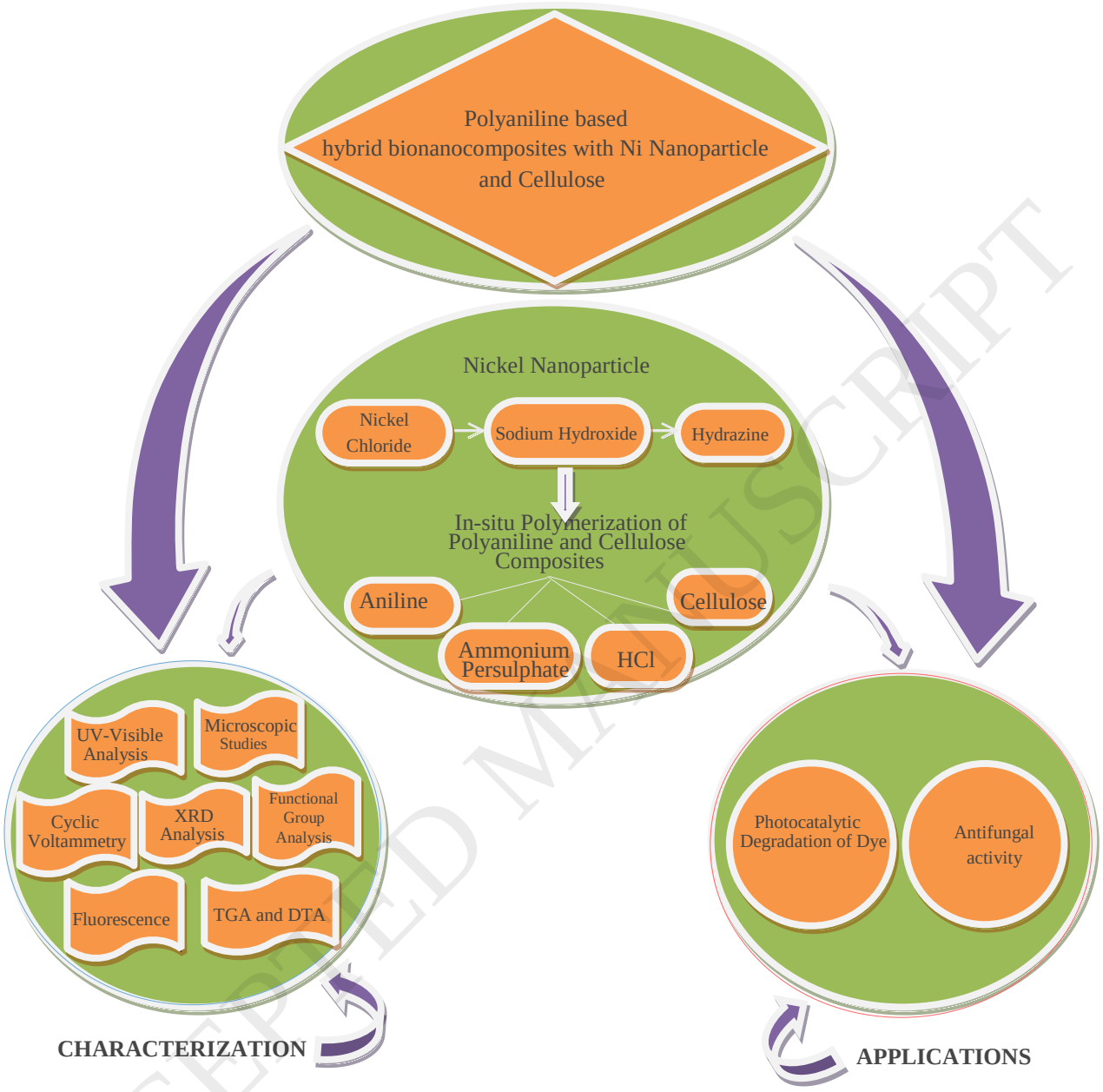

Bio-nanocomposites for the enhanced visible light driven photocatalytic degradation of dye and antifungal activity

ACCEPTED MANUSCRIPT

Highlights:

- Polyaniline based hybrid bio-nanocomposite have been synthesized via in-situ polymerization of aniline with cellulose and Ni nanoparticle.
- Electrochemical double layer capacitance was used to calculate the electrochemical surface area of the bio-nanocomposites.
- Bio-nanocomposites show enhanced photocatalytic activity and anti-fungal activity.
- Fluorescence spectra were used to study charge carrier separation by Photoluminescence intensity.
- Superoxide radicals ($\cdot O_2^-$) and holes (h^+) were found to be the primary reactive species for the photodegradation.

ABSTRACT

Nickel doped polyaniline/cellulose bionanocomposites have been synthesized via in-situ polymerization of aniline and hydrothermally prepared nickel nanoparticles. The as prepared materials were characterized by X-ray diffraction (XRD), fourier transform infrared spectroscopy (FT-IR), ultraviolet-visible (UV-vis) spectroscopy, scanning electron microscopy (SEM), energy dispersive spectroscopy (EDS) and transmission electron microscopy (TEM). Cyclic Voltammetry (CV) was used to determine the electrochemical surface area (ECSA) of the materials by using the electrochemical double layer capacitance (EDLC) data. SEM images reveal that synthesized nanocomposites contain spherical Ni nanoparticles scattered uniformly within PANI-Cellulose matrix. The as prepared materials exhibited significant degradation of reactive orange (RO-16) dye under visible light. Incorporation of Ni nanoparticles in to the polymer matrix causes strong adsorption of dye in case of PANI/C/Ni, PANI/Ni as compared to that of PANI. The photodegradation of RO-16 was achieved by the electron-hole pair separation and formation of reactive species by trapping of the photo generated electron from the surface of photo catalyst. Scavengers were added to identify the primary reactive species. Fluorescence spectroscopy was to study the recombination behavior of charge carriers (electron-hole pair) during photodegradation. Moreover, the anti-fungal nature of the bionanocomposites was also examined and the materials were found to be effective in growth control of two pathogenic fungal strains- *Rhizoctonia solani and Alternaria alternate*.

ACCEPTED MANUSCRIPT

Keywords: Nanoparticle, Visible light, Electron-hole pair, Antifungal, Absorption, Capacitance.

1. INTRODUCTION

Rapid industrial development and heavy production from the industries discharging excessive pollutants (e.g. dyes, drugs and pesticides etc) directly into the water streams and pollute our pristine sources. Presence of azo-dyes is a serious threat to both human health and the environment [1, 2]. Hence, their removal from natural water resources is of outmost importance. Reactive orange 16 (RO-16) dyes are very toxic and reported to cause skin and eye irritation, inhalation problems and even cancer in extreme cases [3,4]. They are widely distributed in the environment due to their high water solubility and thus need immediate treatment [4]. Nanocomposites matrices have emerged as efficient photocatalyst for the treatment of waste water containing dyes [5, 6]. Moreover these nanocomposites are also useful for the removal of toxic heavy metals such as lead, copper, chromium, cadmium, mercury and zinc etc [7, 8]. These nanocomposites are also useful in allied areas like fabrication of solar panels, light emitting diodes, displays, batteries and sensors, electromagnetic shielding, actuators, microelectronic devices and are quite effective as antibacterial or antifungal agents [9,10].

Over the past few decades a number of hybrid nanocomposites consisting of semiconductor nanoparticles such as ZnO, CdS, WO_3, BiOBr along with conducting polymer such as polypyrrole, polyaniline, polythiophene have been synthesized and used extensively in the photocatalytic degradation of dyes sensitive to both UV (>3.0 eV bandgap) and Visible light (<3.0 bandgap) [11]. However, limited solubility and non-biodegradability are limiting the use of conducting polymers. The problem of non biodegradable nature of these conducting polymers can be solved by grafting a conducting polymer on to a biopolymer chain like cellulose, chitosan etc [12].

Among these conducting polymers, PANI due to its high conducting properties compared to metals, has attracted much attention towards energy storage, sensors and electrochromic devices [13]. PANI has shown high absorptivity and excellent redox property which make it useful in

ACCEPTED MANUSCRIPT

photodegradation [14-16]. The photocatalytic activity of PANI can be further enhanced by doping it with nanomaterials. Semiconductor nickel nanoparticles due to their chemical stability have been used in electroplating, batteries, proton exchange membrane, fuel cell, sintering additives and in nanowires [17, 18]. They are also used as a photocatalyst for the degradation of dyes (Methylene blue, Rhodamin B etc) [19, 20]. Conducting polymer based Ni nanocomposites have already been studied by various groups. Polyaniline-Ni nanocomposites have been used as supercapacitor [21] while polythiophene-Ni nanocomposites have been used as a semiconductor [22].

Cellulose being most abundant organic biopolymer with high biocompatibility is used in cosmetics, food, pharmaceuticals etc. It has also been used to improve the adsorption of dye on the catalyst [23, 24]. Thus, a combination of conducting biopolymer with Ni nanoparticles may have a synergistic effect that dramatically improves the photocatalytic activity of Ni nanoparticles as it promotes the adsorption of dye on the photocatalyst surface [25-27]. To the best of our knowledge, no report is available in literature on the photocatalytic properties of PANI/Cellulose/Ni bionanocomposites.

Thus the main aim of the work is to prepare novel bionanocomposites containing a conducting biopolymer with Ni nanoparticle (Polyaniline/Cellulose/Nickel or PANI/C/Ni). The materials were used for visible light driven photocatalytic degradation of textile azo-dye reactive Orange-16 (RO-16). Apart from the potential application in the photodegradation of RO-16, the materials were also tested for fungicidal properties against two pathogenic fungal strains in order to use the bionanocomposites in packaging food stuff.

2. Experimental

2.1. Materials and Reagents

All chemical used in the present work were of analytical grade. Hydrazine was purchased from Thermo Fisher Scientific India while Ethylene glycol (anhydrous) and hydrochloric acid were purchased from Sigma-Aldrich (USA). Sodium hydroxide purified and Nickel chloride hexahydrate were procured from Merck Specialties Pvt.Ltd (Germany). Aniline LR, ammonium persulphate and cellulose was purchased from S.D. Fine-chem Ltd (India).

ACCEPTED MANUSCRIPT

2.2. Synthesis of bionanocomposite materials

2.2.1. Synthesis of nickel nanoparticles

Nickel nanoparticles were synthesized by the reduction of Ni (II) salt with hydrazine in alkaline conditions. A solution of 0.15mM nickel chloride was prepared in 50 ml of ethylene glycol and NaOH(1.0 M) and hydrazine (0.5M) prepared in distilled water were added in a sequence to nickel chloride solution and kept in a hydrothermal reactor. The hydrothermal reactor was then placed in a furnace for 10 h at 60 °C. The following reaction took place in the reactor:

$$2Ni^{2+} + N_2H_4 + 4OH^- \longrightarrow 2Ni + N_2 + 4H_2O$$

In the above reaction, Ni (II) was reduced to Ni (0) in presence of hydrazine as a reducing agent. After 10 h, the hydrothermal reactor was taken out of the furnace and allowed to cool at room temperature. The samples were washed with acetone and distilled water and kept for drying in oven (60 °C) for 2 h [28].

2.2.2. Synthesis of polyaniline

Polyaniline was synthesized by the chemical oxidative polymerization of aniline monomer using ammonium persulphate as oxidant. Ammonium persulphate (0.1 M) was prepared in distilled water and was added drop wise to aniline (0.1 M) prepared in HCl. Prior to this aniline solution was stirred for 15 min. A deep green precipitate was obtained which was then filtered manually, washed with distilled water and acetone and dried at room temperature [5].

2.2.3. Synthesis of PANI/C/Ni bionanocomposites

Polyaniline was synthesized from aniline and ammonium persulphate as discussed in the previous section. However, the bionanocomposites was prepared by adding 0.1g of cellulose and 0.1g of nickel nanoparticle to aniline solution (.1M) during its in situ polymerization. The aniline solution was stirred for 15 minutes before adding cellulose and Ni nanoparticle in a sequence followed by drop wise addition of ammonium persulphate under constant stirring. The greenish blue precipitate thus obtained was filtered, washed with copious amount of distilled water and acetone. The washed samples were finally dried at room temperature [5, 28].

2.3. Characterization of as prepared materials

ACCEPTED MANUSCRIPT

X-ray diffraction pattern was drawn at room temperature with Shimadzu XRD 6100-X-ray diffractometer. Functional group analysis of the as prepared materials has been carried out using FTIR spectrometer (Perkin Elmer Spectrum Two USA) in the range 4000-500 cm^{-1}. Thermogravimetric and differential thermal analysis (Shimadzu DTC-60H Japan) have been carried out to ensure the thermal stability of the sample. Surface morphology and quantitative analysis of the elements of the as prepared materials was probed by scanning electron microscope (SEM) coupled with energy dispersive X-ray spectroscopy (EDX) (SEM, EDX, JOEL Japan) while the size and shape of the particles were studied by transmission electron microscope (TEM JOEL Japan). UV–Visible spectrophotometer (Shimadzu UV-Vis 1601 Japan) was used to measure the residual concentration of azo dye (RO-16) during photodegradation while UV-Vis-NIR spectrophotometer (Perkin Elmer Lambda 35 USA) equipped with an integrating sphere assembly was used to obtain diffuse reflectance of the sample in the region of 300-800 nm. The recombination of charge carriers during photodegradation was estimated from the fluorescence emission spectra drawn in the wavelength range of 300-600 nm using Shimadzu Spectrofluorometer 5000, (Japan) ($\lambda_{excitation}$ is 420nm).

2.4. Cyclic Voltammetry and sample fabrication

Cyclic Voltammetry was performed to investigate the electrochemical surface area (ECSA) by measuring the electrical double layer capacitance (EDLC) of the bionanocomposites using three electrode systems (Autolab 204, Netherland). The system employed Ag/AgCl as reference electrode, Pt as counter electrode and Glassy carbon electrode (GCE) contains the as prepared material, as working electrode in the potential range of +1.2 to -1.2V vs Ag/AgCl and 1MKOH solution was taken as an electrolyte. The sample fabrication was performed in accordance with Saquib et al [29]. Briefly, 3 mg of the catalyst was taken along with 0.5 ml of each isopropyl alcohol (IPA) and water respectively while chitosan solution with glacial acetic acid was used as binder [30]. The prepared solution was deposited on polished glassy carbon electrode and dried for 30 min. The solution was purged with N_2 gas to create inert atmosphere prior to electrochemical analysis.

2.5. Photocatalytic activity and determination of reactive species

ACCEPTED MANUSCRIPT

Photocatalytic activity of the as prepared PANI, PANI/Ni and PANI/C/Ni was assessed by examining the photodegradation of RO-16 in a visible photoreactor made up of pyrex glass and equipped with tungsten lamp (intensity 500 W). The contents of the reactor were stirred continuously using a magnetic bar and an oxygen pump was employed to provide molecular oxygen. The temperature of the photoreactor was controlled by using refrigerated circulating bath. An appropriate amount of the photocatalyst (0.1 g) was taken per 100 ml of the dye solution in the reactor. Prior to irradiation the solution was stirred for 20 min in the dark to attain the adsorption-desorption equilibrium between the dye and photocatalyst. Thereafter, the solution was irradiated and samples were collected periodically to measure the residual concentration of the RO-16 by UV-Visible spectrophotometer (λ_{max} 493 nm). The dye degradation efficiency of the photocatalyst was calculated using the following formula:

$$\text{Degradation efficiency} = \frac{(C_0 - C_t)}{C_0} x100\ (\%) \qquad (1)$$

where C_0 is the initial concentration and C_t is the concentration at time‘t’. Further to identify the primary reactive species responsible for the photodegradation of the dye, various scavengers were used as trapping agent to quench the reactive species. 2 mM each of t-butyl alcohol (TBA), p-benzoquinone, and ethylenediaminetetraacetic acid (EDTA) was used in separate experiments to quench $^{\cdot}OH$, $^{\cdot}O_2^-$ and h^+ respectively [31]. The scavengers were added to the dye solution before the addition of photocatalyst.

2.6. Antifungal test

Two pathogenic fungal strains-*Rhizoctonia solani* and *Alternaria alternata,* were obtained from Microbial Type culture collection (IMTECH Chandigarh India). The strains were cultured on PDA (Potatoe Dextrose Agar) at 27°C in the dark. Anti-fungal tests were performed by the agar dilution method with some modification [32]. Conducting biopolymer (PANI/C) and bionanocomposites (PANI/C/Ni) at a concentration of 0.5, 1.0, 1.5, 2.0 (mM) were mixed with PDA media while composite free PDA served as control. The test and control media were poured onto the sterile petri dishes (9cm diameter) and the fungal strains were inoculated after the PDA media solidified. A disc (1.4cm) of fungal mycelial material taken from the edge of 7-day-old fungal cultures and was placed in the centre of each petridish followed by parafilm sealing to

ACCEPTED MANUSCRIPT

prevent dehydration. The treated and untreated petri dishes were then incubated at 27°C. The efficacy of as prepared composites was evaluated in terms of percent inhibition of fungal colonies after 12 days of incubation by measuring the diameter of fungal colonies and using the formula given below [33]. Different authors have used different methods (such as disc diffusion method or broth diffusion method) to study the antifungal activity of nanoparticles. Disc-diffusion method is more used to study antibacterial activity but Khan et al. 2014 [33] have studied the antifungal activity of ZnO nanoparticles with a little modification. Kim et al 2008 [34] studied the efficacy of Ag nano particles on *Ascomycetous fungi* (*in-vitro*) causing wilting of oak. The method used in the present study for antifungal test is simple and economical and can be applied to study the efficacy of nanoparticles, fungicides and essential oil [32]. All tests were performed in triplicate and the values were expressed in centimeters.

$$\text{Per cent (\%) Inhibition} = \frac{Diameter\ of\ control\ colony - diameter\ of\ treated\ colony}{Diameter\ of\ control\ colony} \text{x } 100 \qquad (2)$$

3. RESULTS AND DISCUSSION

3.1. X-ray diffraction

The crystal structure and particle size of as-prepared PANI, PANI/Ni and PANI/C/Ni have been determined by powder X-ray diffraction as shown in Fig.1. The diffractograms of the PANI shows a broad hump appearing at around 2θ value of 25.6º with corresponding *hkl* values of (2,0,0) and a sharp peak at 15.6º with *hkl* values of (0,1,1). The diffraction pattern of PANI/C/Ni can be categorized in 2θ value of 25.50º, 29.40º with corresponding *hkl* values of (2,0,0) and (0,0,2) respectively, indicating the crystalline nature of bionanocomposites, where as in case of PANI/Ni the diffraction peaks shown at 2θ values are 17.20º,19.80º, 26.0º, 30.0º, 36.4º,41.2º corresponds to *hkl* values of (0,0,1),(1,0,0),(2,0,0),(0,0,2), (1,1,0),(1,1,1) respectively. Upon the incorporation of cellulose and Ni nanoparticles to the PANI, broad peaks appearing in PANI converted into sharp peaks and showing improvement in crystalline nature which is due to the angle of strains. The average crystal size of the composites was calculated by using Debye-Scherer formula given below [36, 37].

$$d = \frac{0.9\lambda}{\beta Cos\theta} \qquad (3)$$

ACCEPTED MANUSCRIPT

Where d is the average crystal size, λ is the X-ray wavelength, β is the full width of the half maxima measured in radians on the 2θ scale and θ is the Bragg's angle for diffraction peaks. The average crystallite size of the matrix was found to be around 58 nm, 50 nm and 223 nm for PANI/Ni, PANI/C/Ni and PANI respectively which shows that the as prepared bionanocomposite was in the nanorange (50 nm)

3.2. Functional group analysis

The FTIR spectra of the synthesized materials PANI, PANI/Ni, PANI/C/Ni and C/Ni are presented in Fig.2. The characteristic peak appearing at 3487 cm^{-1}corresponds to the stretching vibration of N-H group of PANI while the peaks in the region 3050-3150 cm^{-1} corresponds to aromatic =C–H group of the PANI. The peaks appearing in the region 2800-2950 cm^{-1} corresponds to aliphatic C–H group while those appearing in the region 1600-1450 cm^{-1} indicate the presence of aromatic ring of PANI. The peaks near 432 $cm^{-1}$are assigned to Ni nanoparticles [21]. Peaks in the region 1300-1050 cm^{-1} are due to –C–O bond in cellulose while those at 3300-3550 cm^{-1} indicate the presence of -O-H group [25, 38]. The peaks of the PANI got more intense and shifted to higher side due to the interaction of PANI with Ni nanoparticles and cellulose [39].

3.3. Thermal analysis

The thermogravimetric and differential thermal analysis of the as prepared materials PANI/Ni and PANI/C/Ni was carried out under nitrogen atmosphere in the temperature range of 0-800°C and the thermograms are presented in Fig.3 (Fig. 3a TGA Curve and Fig. 3b DTA Curve). The results showed weight loss of PANI/C/Ni in three different regions in the TGA curve. The first weight loss of the curve in the temperature range of 55-210°C corresponds to the evaporation of physical water adsorbed on to the surface of the nanocomposites while the second loss in the range of 210-400°C corresponds to the removal of lattice water. The final weight loss above 400°C is due to the decomposition of the polymeric part i.e. cellulose and PANI [26, 40]. The thermal stability of PANI has been reduced upon incorporation of cellulose. The percent weight loss of the bionanocomposites (PANI/C/Ni) observed at the mid-point (157.30, 308.40, and 506.63) is 1.503, 2.506, and 4.950% respectively, and the weight loss of the nanocomposites (PANI/Ni) observed at mid-point (217.09, 447.25, 604.41) was found to be 1.202, 1.870, and

ACCEPTED MANUSCRIPT

2.047% respectively. Moreover, the DTA curve show an endothermic peak in the temperature range of 80-210°C for both the samples attributed to loss of physically and chemically absorbed molecular water and hydroxyl groups. The second peak in the DTA curve is due to weight loss in region 210-350°C and the final broad exothermic peak between 345-700°C corresponds to decomposition of hydroxides leading to the shrinkage of the material through crystallization [41].

3.4. Microscopic studies with SEM, TEM and EDS

Surface morphology of the materials has been studied by microscopic studies. SEM micrograph in Fig.4a, b showed the uniform distribution of Ni nanoparticle and cellulose (white color) with in the dark colored polyaniline. The micrographs of PANI/Ni are quite irregular in shape as shown in Fig.4c but Ni nanoparticle shows good uniformity with PANI [26]. The pores appearing in the PANI/C/Ni are attributed to uniform deposition of Ni nanoparticle onto PANI surface. Porosity of the nanocomposites results into higher photocatalytic activity due to higher surface area of the material [42]. Cellulose biopolymer mixed well with the prepared nanocomposites but in irregular fashion as shown in Fig.4a, b. The elemental composition and the purity of the as prepared samples were ascertained with the help of energy dispersive x-ray spectroscopy and the results are presented in Fig.5a whereas the quantitative results of the elemental composition are shown in Fig.5b.

TEM images of the PANI/Ni and PANI/C/Ni are shown in Fig.6. Micrographs shows well dispersed nanorange nickel nanoparticles bonded to PANI matrix. From the images, it is clear that the white color appearing on the boundaries is attributed to cellulose. Upon the incorporation of the Ni nanoparticle the matrix seem to be closely bonded to each other with even smaller size of the particles shown in Fig.6b.The nanorange image of the nanocomposites are presented in Fig.6c and the size of the nanocomposites are in accordane with results obtained from XRD and found to be in the nanorange as calculated by the scherrer's formula.

3.5. Electrochemical surface area

The electrochemical surface area (ECSA) of the as prepared materials has been determined using cyclic voltammetry. The ECSA was calculated from the electrochemical double layer

ACCEPTED MANUSCRIPT

capacitance (EDLC) method. EDLC was measured from cyclic voltammograms of the materials drawn in the region -1.2 to 1.2V vs (Ag/AgCl) in 0.1M KOH [29] (Fig.1S, Supplementary Information). In order to calculate the ECSA from EDLC, the cyclic voltammetry was again performed in the region 0.1 to 0.2V with varying scan rates (ranging from 10 to 80 mVs^{-1}) as shown in Fig. 7a.

The value of the linear slope obtained from the EDLC was used to represent the electrochemical surface area as shown in Fig. 7b. The electrochemical surface area of PANI, PANI/Ni and PANI/Ni/C was found to be 0.000635 $mFcm^{-2}$, 0.00108 $mFcm^{-2}$ and 0.00149 $mFcm^{-2}$ respectively. Thus the ECSA of PANI/C/Ni was found to be higher than that of PANI as well as PANI/Ni nanocomposites which promotes better degradation of the dye molecule by the resulting bionanocomposites. This is due to the higher adsorption of the dye on the enhanced surface of the bionanocomposites [43]. So it can be concluded that ECSA greatly affect the photocatalytic activity.

3.6. UV-diffuse reflectance spectra

The band gap values of PANI, PANI/C and PANI/C/Ni were calculated from UV-diffuse reflectance spectra. Band gap was calculated by using the following relation:

$$(h\nu.\alpha) = (Ah\nu\text{-}Eg)^{n/2} \qquad (4)$$

where α is the proportionality constant to kubelka Munk function F(R), then the expression becomes,

$$\{(h\nu.F(R)\} = (Ah\nu\text{-}Eg)^{n/2} \qquad (5)$$

Where ν is the frequency of light, F(R) is the kubelka Munk function; A is the proportionality constant and Eg is the band gap energy. The value of n is determined by the type of optical transition (n=1 for direct transition and n=4 for indirect transition). In the present case, the value of n is taken as 1 for direct optical transition $(F(R)\ h\nu)^{1/2}$ $(eV)^2$ vs. Eg (eV) [44, 45]. The band gap value for PANI was found to be 2.1 eV which is quite similar as reported elsewhere [46] and upon the doping of the Ni nanoparticle and cellulose the bandgap of PANI has been shifted towards the lower value (Fig. 8a). Absorption spectra of materials in the region 200-700 nm Fig.

ACCEPTED MANUSCRIPT

8b represents the. The materials show strong absorption in the region 450-500 nm and higher absorption coefficient in case of PANI/C/Ni. Lower bandgap and higher absorption of the PANI/C/Ni bionanocomposites are responsible for the higher photocatalytic activity [47].

3.7. Photocatalytic activity and kinetics of photodegradation

The photocatalytic activity of the semiconductor depends upon the bandgap potential of valence and conduction band. The valence band and conduction band edge potential of PANI was calculated by the formula:

$$E_{VB} = X - E^c + 0.5\ Eg \qquad (6)$$

$$E_{CB} = E_{VB} - Eg \qquad (7)$$

Where X is the electronegativity of the material expressed as the geometric mean of the electronegativity of the constituent element, E^c is the energy of the free electron on hydrogen scale (4.5 eV) and Eg is the band gap energy. The conduction band and valence band and potential of PANI were found to be -1.3 and 0.8 eV [46].

The photocatalytic degradation of RO-16 dye was evaluated using the as prepared materials as catalyst and the results are presented in Fig.9a. Upon visible irradiation PANI is excited and generates electron-hole pairs in HOMO (highest occupied molecular orbital) and LUMO (lowest unoccupied molecular orbital) respectively. The electrons of LUMO of PANI flow easily toward 'Ni' nanoparticles scattered on the surface of PANI *via* schottky barrier which is consistent with the previous studies on electron transfer from semiconductor to metal nanoparticles [48]. It can reduce the recombination of electron-hole pairs and increase the lifetime of the charge carriers. The photoexcited electrons of 'Ni' nanoparticles as a result of SPR (surface Plasmon resonance) effect together with the electrons transferred from PANI convert the molecular oxygen to superoxide $\cdot O_2^-$. Meanwhile the holes in the HOMO of PANI will react with the water molecule and produce $OH^{\cdot}$ radicals. Now the reactive species generated in the redox process h+, $O_2^{\cdot -}$ and $^{\cdot}OH$ would directly mineralize the dye molecules into degradation products. In this way Ni nanoparticles help in efficient separation of charge carriers which increases the life time of charge carriers. High bandgap cellulose incorporated in to the PANI/Ni nanocomposites assist in minimizing the recombination rate of the charge carriers in the resulting bionanocomposites and

ACCEPTED MANUSCRIPT

favor higher absorption of the dye molecule on to the surface of the catalyst. Based on the above discussion, the following reactions might have occurred during the photodegradation of RO-16.

$$\text{PANI/C/Ni} \xrightarrow{h\upsilon} h^+(\text{PANI/C})\ e^-(\text{Ni}) \quad (8)$$

$$h^+ + H_2O \longrightarrow {}^{\cdot}OH \quad (9)$$

$$e^- + O_2 \longrightarrow {}^{\cdot}O_2^- \quad (10)$$

$$h^+/{}^{\cdot}OH/{}^{\cdot}O_2^- + \text{RO-16} \longrightarrow \text{Degradation product} \quad (11)$$

The photocatalytic activity of PANI/C/Ni ternary composite, PANI/C and PANI was calculated from residual concentration of RO-16 dye by using UV- spectrophotometer [3, 49-50]. The kinetics of the photocatalytic degradation of the dye was studied by plotting residual concentration of RO-16 dye as C/C_0 vs. irradiation time as shown in Fig. 9b and the straight line plot shows pseudo first order kinetics has been followed.

$$\frac{C}{C_0} = e^{-kt} \quad (12)$$

$$ln\left[\frac{C}{C_0}\right] = -kt \quad (13)$$

where C_0 is the initial concentration and C is the concentration of the dye after time‘t’. The experiment shows that significant degradation of RO-16 has been occurred in presence of PANI, PANI/Ni photocatalyst and higher degradation was observed in case of PANI/C/Ni bionanocomposites. The rate constant was found to be 0.049 min^{-1}, 0.064 min^{-1}, 0.08 min^{-1} and 0.00072 min^{-1} for PANI, PANI/Ni, PANI/C/Ni and control samples (without photocatalyst) respectively. The percent dye degradation efficiency was found to be 93% with PANI/C/Ni catalyst during the test duration of 55 min. A possible mechanism of the photocatalytic degradation of RO-16 has been presented in Fig. 9c and a comparative study of the photocatalytic degradation of dye in presence of different polyaniline based nanocomposites is given in Table 1.

ACCEPTED MANUSCRIPT

The recombination rate of the charge carriers was further studied by measuring the PL intensity using fluorescence spectroscopy. Low recombination rate of the charge carrier minimizes the PL intensity and maximizes the photocatalytic activity of the catalyst. The PL intensity of the PANI/C/Ni bionanocomposites was found to be lowest among the test sample PANI, PANI/Ni and PANI/C/Ni as shown in Fig. 10. Thus the photocatalytic activity of the PANI/C/Ni is highest which is in good agreement with the results of the photocatalytic activity of the samples (section 3.7).

3.8 Study of scavengers

To identify the primary reactive species involved in the photodegradation of RO-16 in the present study, different scavengers were used as trapping agents. From the Fig.11, it is clearly seen that the addition of tertiary butyl alcohol (as trapping agent to quench ·OH) has no significant effect on the rate of photodegradation however addition of p-benzoquinone and EDTA to quench $\cdot O_2^-$ and h^+ respectively reduces the rate of photodegradation appreciably. Thus it can be concluded that $\cdot O_2^-$ and h^+ were the primary reactive species for the photodegradation of RO-16 while ·OH was not the primary reactive species for the photodegradation in the present study. A tabular representation of the properties of as prepared materials PANI, PANI/Ni and PANI/C/Ni are given in Table 2.

3.9. Antifungal tests

At the end of the study, the materials (PANI/C and PANI/C/Ni) were tested for antifungal activity against two pathogenic fungal strains viz, *Rhizoctonia solani* and *Alternaria alternate* and the results are presented in Fig. 12. The test for antifungal activity of materials was carried out at different concentration viz; 0.5, 1.0, 1.5, 2.0 mM of PANI/C/Ni. The medium with 0.5 mM of PANI/C/Ni showed 42 % greater inhibition of *R. solani* than PANI/C ($P \leq 0.05$) while the bionanocomposite showed 50 % greater inhibition of *A. alternate* than PANI/C ($P \leq 0.05$). Thus, bionanocomposite PANI/C/Ni was found to be causing greater inhibition of fungal growth than PANI/C. On comparing, PANI/C/Ni showed 80% greater inhibition than PANI/C. Alternatively, it can be concluded that PANI/C is biodegradable compared to PANI/C/Ni and the fungicidal effect of Ni nanoparticle can easily be understood from Fig. 12. The simple photographic images of inhibited colonies of *Rhizoctonia solani* (causing sheath blight of *Oryza sativa*) and *Alternaria*

ACCEPTED MANUSCRIPT

*alternate (*causing leaf blight of *Withania somnifera)* are shown in Fig. 2S (Supplementary Information).

4. Conclusions

PANI/C/Ni bionanocomposites was successfully synthesized by chemical oxidative polymerization. The polyaniline based nanocomposites showed a strong synergistic effect of polyaniline/C/Ni on photocatalytic activity and the recombination rate and thus it can be effectively used for the photodegradation of the dyes as compared to the previous studies. Electrochemical surface area of the as prepared materials determined by the electrical double layer capacitance found to be higher in case of PANI/C/Ni that simultaneously increases the photocatalytic activity by providing larger surface area. The rate constant for PANI/C/Ni is significantly higher than both pure PANI and PANI/Ni due to greater separation of photogenerated charge carriers (low charge carrier recombination). The incorporation of cellulose to PANI/Ni minimizes the bandgap and enhances adsorption of the dye molecule on catalyst surface which further enhances the rate of photodegradation. The bionanocomposite was found to be quite stable up to 300ºC. The incorporation Ni in to the PANI/C chains improves the fungicidal properties of the conducting biopolymer remarkably. Thus, it can be concluded that the as prepared bionanocomposite can be used as excellent photocatalyst in the treatment of water as well as fungicidal agent in the packaging of food stuffs.

Acknowledgements

Authors are thankful to Department of Chemistry for providing necessary research facilities. University Sophisticated Instrumentation Facility is duly acknowledged for providing facilities for SEM and TEM.SS also thanked UPCST for providing financial assistance for this work.

ACCEPTED MANUSCRIPT

References

[1] A. Rajeswari, S. Vismaiya, A. Pius, Preparation, characterization of nano ZnO-blended cellulose acetate-polyurethane membrane for photocatalytic degradation of dyes from water, Chem. Eng. J. 313 (2017) 928-937.

[2] S. Natarajan, H.C. Bajaj, R.J. Tayade, Recent advances based on the synergetic effect of adsorption for removal of dyes from waste water using photocatalytic process. J. Environ. Sci. 65 (2018) 201 – 222.

[3] N. Ahmad, S. Sultana, A. Azam, S. Sabir, M.Z. Khan, Novel bionanocomposite materials for enhanced biodegradability and photocatalytic activity, New J. Chem. 41(18) (2017) 10198-10207.

[4] S. Sultana, M.D. Khan, S. Sabir, M.K. Gani, M. Oves, M.Z. Khan, Bio-electro degradation of azo-dye in a combined anaerobic–aerobic process along with energy recovery. New J. Chem. 39(12) (2015) 9461–9470.

[5] S. Sultana, N. Ahmad, S.M. Faisal, M. Owais, S. Sabir, Synthesis, characterisation and potential applications of polyaniline/chitosan-Ag-nano-biocomposite, IET Nanobiotechnol. 11(7) (2017) 835-842.

[6] Y. Zhang, F. Gao, B. Wanjala, Z. Li, G. Cernigliaro, Z. Gu, High efficiency reductive degradation of a wide range of azo dyes by SiO_2-Co core-shell nanoparticles, Appl. Catal. B: Environ. 199 (2016) 504-513.

[7] S.U. Khan, I.H. Farooqi, S. Ayub, Studies on application of Fe based binary oxide nanoparticles for treatment of lead (Pb^{2+}) contaminated water-A batch study, Mater. Today: Proceedings. 4(9) (2017) 9650-9655.

[8] N.A. Khan, K.A. Khan, M. Islam, Water and Wastewater Treatment using Nano-technology" Chemistry of Phyto potentials: Health, Energy and Environmental Perspectives, Springer, Berlin Heidelberg, Section C. (2012) 315-318.

[9] K.P.O. Mahesh, D.H. Kuo, Synthesis of Ni nanoparticles decorated SiO_2/TiO_2 magnetic spheres for enhanced photocatalytic activity towards the degradation of azo dye, Appl. Surf. Sci. 357 (2015) 433-438.

[10] X. Li, C. Zhang, T. Meng, Synergistic effects from graphene oxide nanosheets and TiO_2 hierarchical structures enable robust and resilient electrodes for high-performance lithium-ion batteries, RSC Adv. 6(6) (2016) 4321-4328.

[11] B.M. Pirzada, O. Mehraj, N.A. Mir, M.Z. Khan, S. Sabir, Efficient visible light photocatalytic activity and enhanced stability of $BiOBr/Cd(OH)_2$ heterostructures, New J. Chem. 39(9) (2015) 7153-7163.

[12] S.A. Hassanzadeh-Tabrizi, M.M. Motlagh, S. Salahshour, Synthesis of ZnO/CuO nanocomposite immobilized on γ-Al_2O_3 and application for removal of methyl orange, Appl. Surf. Sci. 384 (2016) 237-243.

ACCEPTED MANUSCRIPT

[13] H. Wang, J. Lin, Z.X. Shen, Polyaniline (PANi) based electrode materials for energy storage and conversion, J. sci: Adv. Mater. Devices, 1(3) (2016) 225-255.

[14] H. Liang, X. Li, Visible-induced photocatalytic reactivity of polymer–sensitized titania nanotube films, Appl. Catal. B: Environ. 86 (2009) 8–17.

[15] F. Duan, Q. Zhang, D. Shi, M. Chen, Enhanced visible light photocatalytic activity of Bi_2WO_6 via modification with polypyrrole, Appl. Surf. Sci. 268 (2013) 129-135.

[16] J. Huang, R.B. Kaner, A general chemical route to polyaniline nanofibers, J. Amer. Chem. Soc. 126(3) (2004) 851-855.

[17] Y. Yu, M. Guo, M. Yuan,W. Liu, J. Hu, Nickel nanoparticle-modified electrode for ultra-sensitive electrochemical detection of insulin, Biosens. Bioelectron. 77 (2016) 215-219.

[18] J.M. Kanold, J. Wang, F. Brummer, L. Siller, Metallic nickel nanoparticles and their effect on the embryonic development of the sea urchin Paracentrotus lividus, Environ. Pollut. 212 (2016) 224-229.

[19] L. Niu, Z. Li, J. Sun, Z. Fan, Y. Xu, P. Gong, J. Wang, Hydrothermal synthesis of Ni@ C core–shell composites with high capacitance, J. Alloys Compd. 575 (2013) 152-157.

[20] J.H. Kim, S.H. Kang, K. Zhu, J.Y. Kim, N.R. Neale, A.J. Frank, Ni–NiO core–shell inverse opal electrodes for supercapacitors, Chem. Comm. 47(18) (2011) 5214-5216.

[21] S.U. Muhamad, N.H. Idris, H.M. Yusoff, M.M. Din, S.R. Majid, In-situ encapsulation of nickel nanoparticles in polypyrrole nanofibres with enhanced performance for supercapacitor, Electrochim. Acta. 249 (2017) 9-15.

[22] P. Pascariu, A. Anton, G. Mircea, V. Loredana, I. Felicia, Metal–polymer nanocomposites based on Ni nanoparticles and polythiophene obtained by electrochemical method, Appl. Surf. Sci. 352 (2015) 95-102.

[23] B.J. Chhetri, D. Soni, A. Bahandur, R. Magar, C.M. Parnell, H. Wayland, F. Watanabe, G. Kannarpady, A.S. Biris, A. Ghosh, Synthesis, characterization, and photocatalytic activity of N-doped carbonaceous material derived from cellulose in textile dye remediation, J. Environ. Chem. Engg. 5(3) (2017) 2586-2596.

[24] W.J. Orts, J. Shey, S.H. Imam, G.M. Glenn, M.E. Guttman, J.F. Revol, Application of cellulose microfibrils in polymer nanocomposites, J. Polym. Environ. 13(4) (2005) 301-306.

[25] X. Wu, Q. Wang, W. Zhang, Y. Wang, W. Chen, Nano nickel oxide coated graphene/polyaniline composite film with high electrochemical performance for flexible supercapacitor, Electrochim. Acta. 211 (2016) 1066-1075.

[26] C. Torres, B. Moreno, E. Chinarro, C. de Fraga Malfatti, Nickel-polyaniline composite electrodes for hydrogen evolution reaction in alkaline media. Int. J. Hydrogen Energy, 42(32) (2017) 20410-20419.

ACCEPTED MANUSCRIPT

[27] J.R. Gomez, F. Monteagudo, A.I.L Lorente, R. Lucena, R. Luque, S. Cardenas, Efficient combined sorption/photobleaching of dyes promoted by cellulose/titania-based nanocomposite films, J. Clean. Prod. 194 (2018) 167-173.

[28] S.H. Wu, D.H. Chen, Synthesis and characterization of nickel nanoparticles by hydrazine reduction in ethylene glycol, J. Colloid Interface Sci. 259(2) (2003) 282-286.

[29] M. Saquib, A. Halder, Ensemble Effect of Ni in Bimetallic PtNi on Reduced Graphene Oxide Support for Temperature- Dependent Formic Acid Oxidation, Chem. Select. 3(14) (2018) 3909-3917.

[30] M. Saquib, A. Halder, Dealloyed Pt_3Co nanoparticles with higher geometric strain for superior hydrogen evolution reaction, J. Solid State Chem. 262 (2018) 229-236.

[31] X. Chen, Z. Wu, D. Liu, Z. Gao, Preparation of ZnO photocatalyst for the efficient and rapid photocatalytic degradation of azo dyes, Nanoscale Res. Lett. 12(1) (2017) 143.

[32] D. Fraternale, L. Giamperi, D. Ricci, Chemical composition and antifungal activity of essential oil obtained from in vitro plants of Thymus mastichina L, J. Essent.Oil Res. 15(4) (2003) 278-281.

[33] J.M. Vincent, Distortion of fungal hyphae in the presence of certain inhibitors. Nature. 159 (1947) 850-850.

[34] S.W. Kim, S.U. Kyoung, L. Kabir, J.K. Young, B.K. Seung, J. Mooyoung, J.S. Sang, S.K. Ha, C. S. Joon, K.K. Jong, S.L. Youn, An In Vitro Study of the Antifungal Effect of Silver Nanoparticles on Oak Wilt Pathogen Raffaeleasp, J. Microbiol. Biotechnol. 19(8) (2009) 760–764.

[35] M.F. Khan, M. Hameedullah, A.H. Ansari, E. Ahmad, M.B.Lohani, R.H.Khan, M.M.Alam, W. Khan, F.M. Husain, I. Ahmad, Flower-shaped ZnO nanoparticles synthesized by a novel approach at near-room temperatures with antibacterial and antifungal properties, Int. J. Nanomedicine. 9 (2014) 853–864.

[36] S. Sultana, M.Z. Khan, K. Umar, Synthesis and characterization of copper ferrite nanoparticles doped polyaniline, J. Alloys Compd. 535 (2012) 44-49.

[37] J. Cao, B. Xu, H. Lin, B. Luo, S. Chen, Chemical etching preparation of BiOI/BiOBr heterostructures with enhanced photocatalytic properties for organic dye removal, Chem. Eng. J. 185 (2012) 91-99.

[38] P. Chen, T.Y. Xiao, Y.H. Qian, S.S. Li, S.H. Yu, A Nitrogen- doped graphene/carbon nanotube nanocomposite with synergistically enhanced electrochemical activity, Adv. Mater. 25(23) (2013) 3192-3196.

[39] K. Cui, Y. Cheng, J. Dai, J. Liu, Synthesis, characterization and microwave absorption properties of $La0.6Sr0.4MnO_3$/polyaniline composite, Mater. Chem. Phys. 138 (2013) 810–816.

ACCEPTED MANUSCRIPT

[40] A. Zakaria, A. Kassim, S.N. Basri, Novel conductive polypyrrole/zinc oxide/Chitosan bionanocomposite: synthesis, characterization, antioxidant, and antibacterial activities, Int. J. Nanomedicine. 10 (2015) 217-227.

[41] W. Raza, M.M. Haque, M. Muneer, T.Harada, M. Matsumura, Synthesis, characterization and photocatalytic performance of visible light induced bismuth oxide nanoparticle, J. Alloys Compd. 648 (2015) 641-650.

[42] B.H. Lee, J.H. Kim, H.S. Yang, Polymerization of aniline on bacterial cellulose and characterization of bacterial cellulose/polyaniline nanocomposite films, Current Appl. Phys. 12(1) (2012) 75-80.

[43] K.M. Girish, S. C. Prashantha, H. Nagabhushana, C. R. Ravikumar, H. P. Nagaswarupa, R. Naik, H.B. Premakumar, B. Umesh, Multi-functional Zn_2TiO_4: Sm^{3+} nanopowders: Excellent performance as electrochemical sensor and UV photocatalyst, J. Sci: Adv. Mater. Devices. 3(2) (2018) 151-160.

[44] B.M. Pirzada, N.A. Mir, N. Qutub, O. Mehraj, S. Sabir, M. Muneer, Synthesis, characterization and optimization of photocatalytic activity of TiO_2/ZrO_2 nanocomposite heterostructures, Mater. Sci. Eng: B. 193 (2015) 137-145.

[45] N. Qutub, B.M. Pirzada, K. Umar, S. Sabir, Synthesis of CdS nanoparticles using different sulfide ion precursors: formation mechanism and photocatalytic degradation of Acid Blue-29, J. Environ. Chem. Eng. 4(1) (2016) 808-817.

[46] J.G. Zhang, H.P. Bi, G.Y. He, Y.W. Zhou, H.Q. Chen, Fabrication of Ag_3PO_4–PANI–GO composites with high visible light photocatalytic performance and stability, J. Environ. Chem. Eng. 2 (2014) 952–957.

[47] W. Dai, H. Xu, J. Yu, X. Hu, X. Luo, X. Tu, L. Yang, Photocatalytic reduction of CO2 into methanol and ethanol over conducting polymers modified Bi_2WO_6 microspheres under visible light, Appl. Surf. Sci. 356 (2015) 173-180.

[48] R. Costi, A.E. Saunders,U. Banin, Colloidal hybrid nanostructures: a new type of functional materials, Angew. Chem. Int. Ed. 49(29) (2010) 4878-4897.

[49] S. Zhang, X. Wang, J. Li, T. Wen, J. Xu, X. Wang, Efficient removal of a typical dye and Cr(VI) reduction using N-doped magnetic porous carbon, RSC Adv. 4(108) (2014) 63110-63117.

[50] O. Mehraj, B.M. Pirzada, N.A. Mir, M.Z. Khan, S. Sabir, A highly efficient visible-light-driven novel pn junction Fe_2O_3/BiOI photocatalyst: Surface decoration of BiOI nanosheets with Fe_2O_3 nanoparticles, Appl. Surf. Sci. 387 (2016) 642-651.

[51] V. Eskizeybek, S. Fahriye, G. Handan, G.Ahmet, A. Ahmet, Preparation of the new polyaniline/ZnO nanocomposite and its photocatalytic activity for degradation of methylene blue and malachite green dyes under UV and natural sun lights irradiations, Appl.Catal.B: Environ. 119 (2012) 197-206.

[52] S. Shahabuddin, M.S. Norazilawati, I.H. Fatem, M.S. Muhammad, M.H. Nay, Synthesis of chitosan grafted-polyaniline/Co_3O_4 nanocube nanocomposites and their

ACCEPTED MANUSCRIPT

photocatalytic activity toward methylene blue dye degradation, RSC Adv. 5(102) (2015) 83857-83867.

[53] V. Gilja, N.Katarina, T.S. Jadranka, H.M.Zlata, K.R. Marijana, Z. Mark, Stability and synergistic effect of polyaniline/TiO_2 photocatalysts in degradation of azo dye in wastewater, Nanomaterials. 7(12) (2017) 412.

[54] M.R. Patil, V. S. Shrivastava, Photocatalytic degradation of carcinogenic methylene blue by using polyaniline-nickel ferrite Nano-composite, Pelagia. Res. Libr. 5(2) (2014) 8-17.

[55] Y. Bu, C. Zhuoyuan, Role of polyaniline on the photocatalytic degradation and stability performance of the polyaniline/silver/silver phosphate composite under visible light, ACS appl. Mater. & interf. 6 (20) (2014) 17589-17598.

[56] M. Aamir, N.A. Muhammad, Y. Ghazala, A. Bashir, F.E. Muhammad, H.Tao, Synthesis and characterization of polyaniline/Zr-Co-substituted nickel ferrite (NiFe1.2Zr0.4Co0.4O4) nanocomposites: their application for the photodegradation of methylene blue, Desalin. Water Treat. 57(26) (2016) 12168-12177.

ACCEPTED MANUSCRIPT

ACCEPTED MANUSCRIPT

FIGURES CAPTION

Fig.1. XRD pattern of the as-prepared materials PANI, PANI/Ni and PANI/C/Ni bionanocomposites.

Fig.2. FTIR spectra of the as prepared polymer nanocomposite and bio-nanocomposites.

Fig.3. Plot of (a) TGA and (b) DTA Curve of the as prepared bio-nanocomposites and nanocomposites matrices.

Fig. 4. SEM images of PANI/C/Ni bio-nanocomposite (a, b) and PANI/Ni nanocomposite (c).
Fig. 5 (a) EDS spectra of as prepared PANI/C/Ni bio-nanocomposite and (b) Quantitative results of the bio-nanocomposites.

Fig. 6. TEM images of PANI/C/Ni bio-nanocomposite (a) and PANI/Ni nanocomposites (b, c).

Fig. 7. (a) Cyclic Voltammograms of the as prepared bio-nanocomposites at different scan rate 10-80 mVs^{-1} and (b) ECSA of the PANI, PANI/Ni and PANI/C/Ni.

Fig. 8. (a)Tauc plots spectra for the band gap calculation of the as prepared materials and (b) UV-DRS absorption spectra of the materials.

Fig.9. (a) Visible spectra of the as prepared materials (b) Kinetics of photodegradation and (c) Probable mechanism for the photodegradation of the RO-16 dye.

Fig.10. Photoluminescence spectra of the samples under investigation.

Fig.11. Effect of scavengers on the photodegradation of dye over bionanocomposite photocatalyst.

Fig.12. Per cent inhibition of fungal growth in presence of PANI/C and PANI/C/Ni.

ACCEPTED MANUSCRIPT

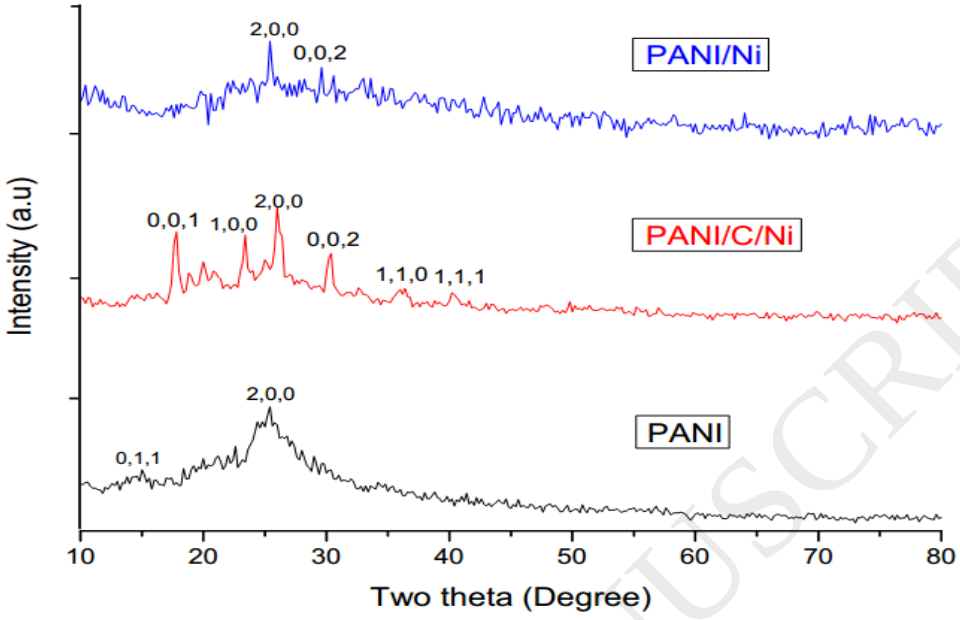

Fig.1. XRD pattern of the as-prepared materials PANI, PANI/Ni and PANI/C/Ni bio-nanocomposites.

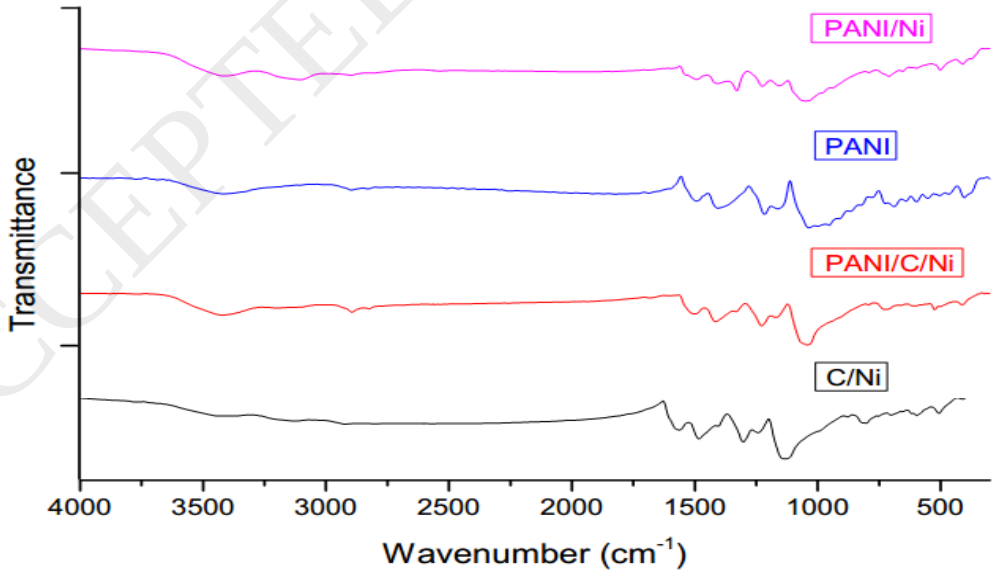

Fig.2. FTIR spectra of the as prepared polymer nanocomposite and bio-nanocomposites.

ACCEPTED MANUSCRIPT

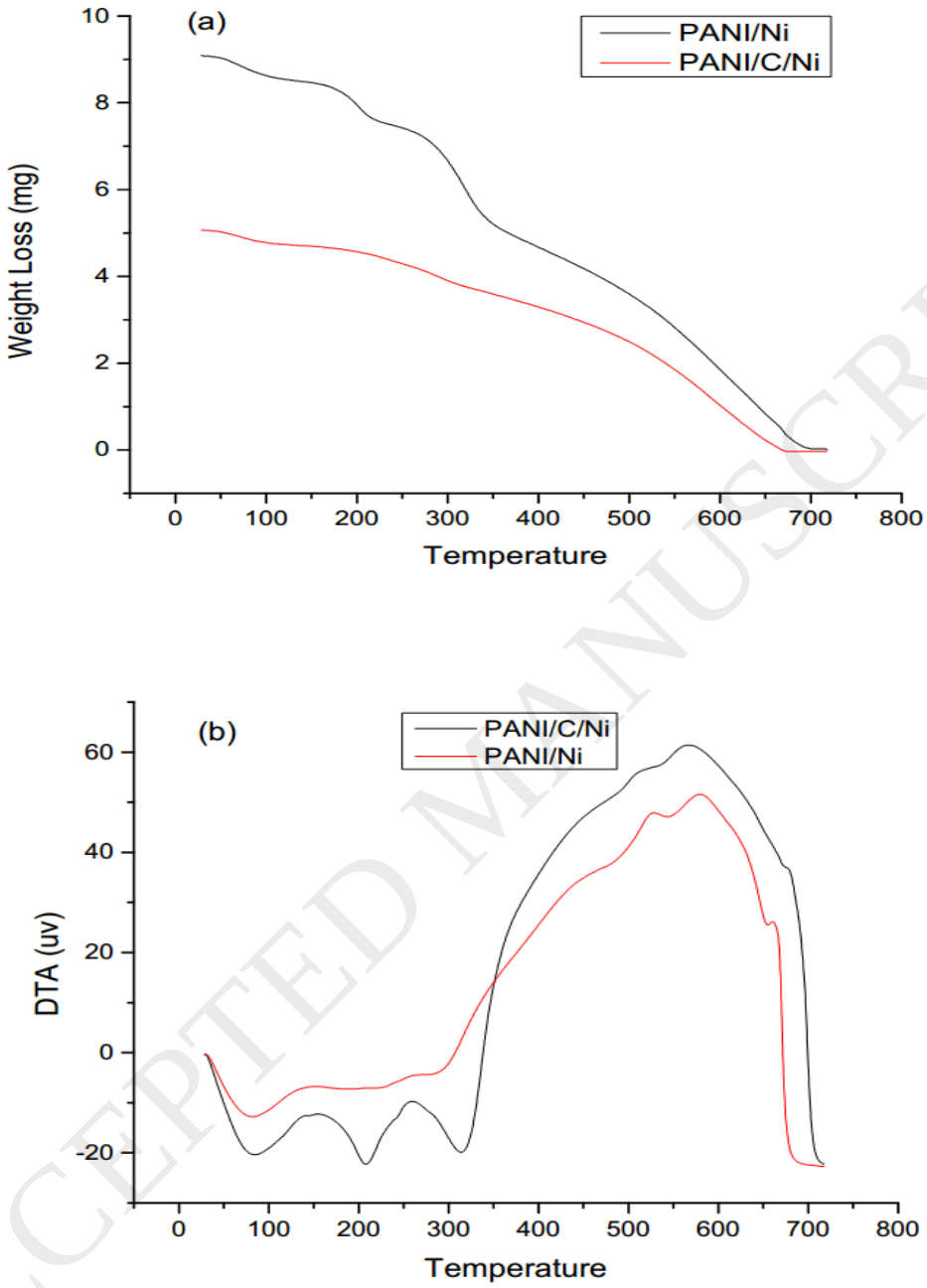

Fig.3. Plot of (a) TGA and (b) DTA Curve of the as prepared bio-nanocomposites and nanocomposites matrices.

ACCEPTED MANUSCRIPT

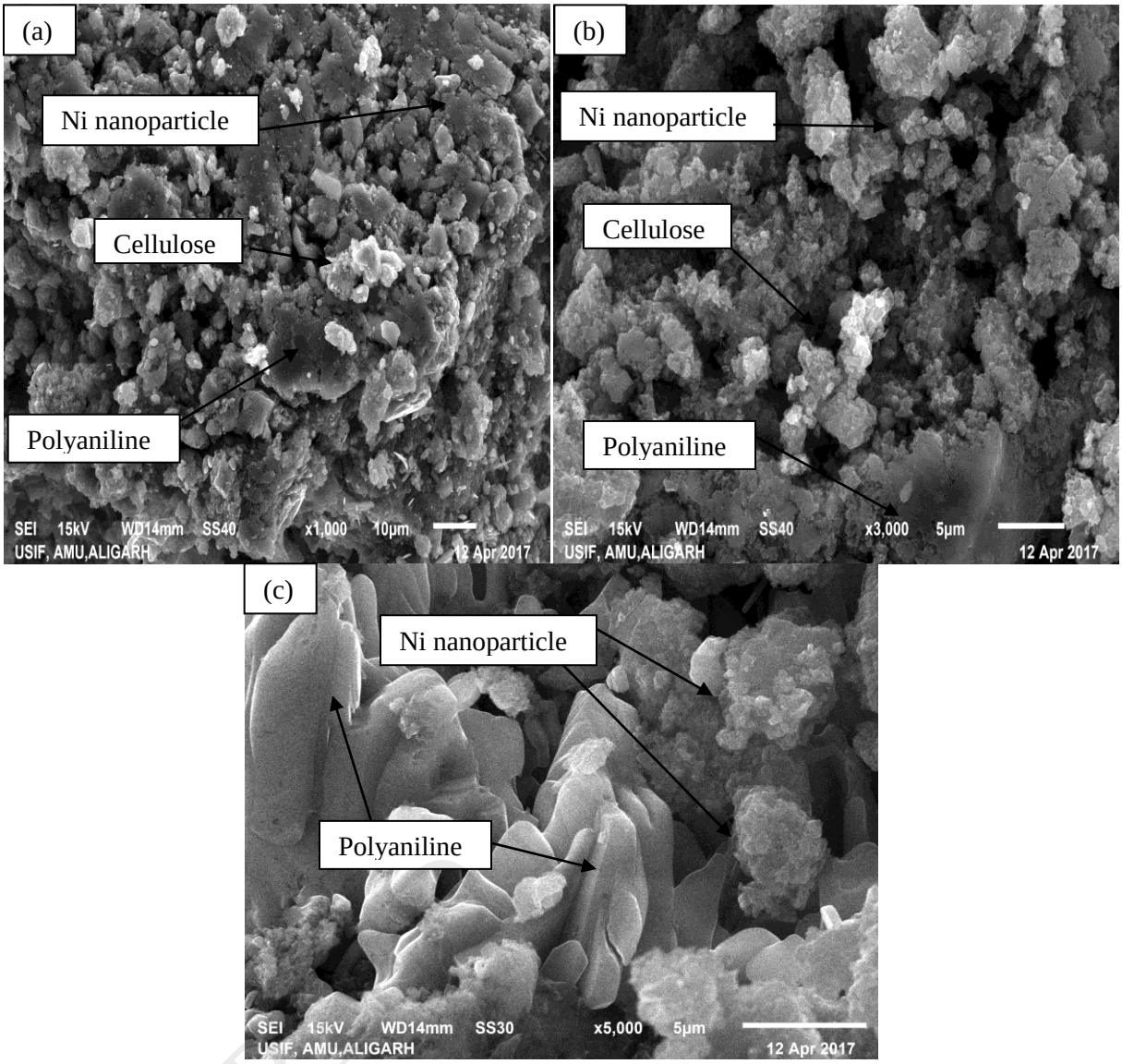

Fig. 4. SEM images of PANI/C/Ni bio-nanocomposite (a, b) and PANI/Ni nanocomposite (c).

ACCEPTED MANUSCRIPT

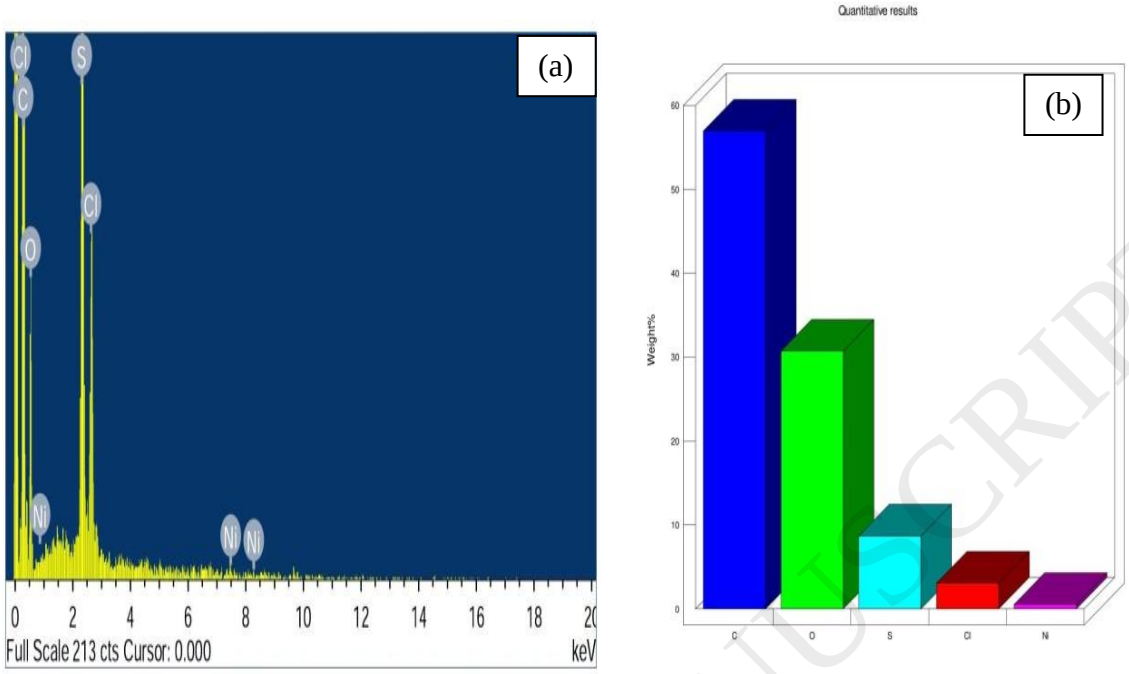

Fig. 5 (a) EDS spectra of as prepared PANI/C/Ni bio-nanocomposite and (b) Quantitative results of the bio-nanocomposites.

ACCEPTED MANUSCRIPT

ACCEPTED MANUSCRIPT

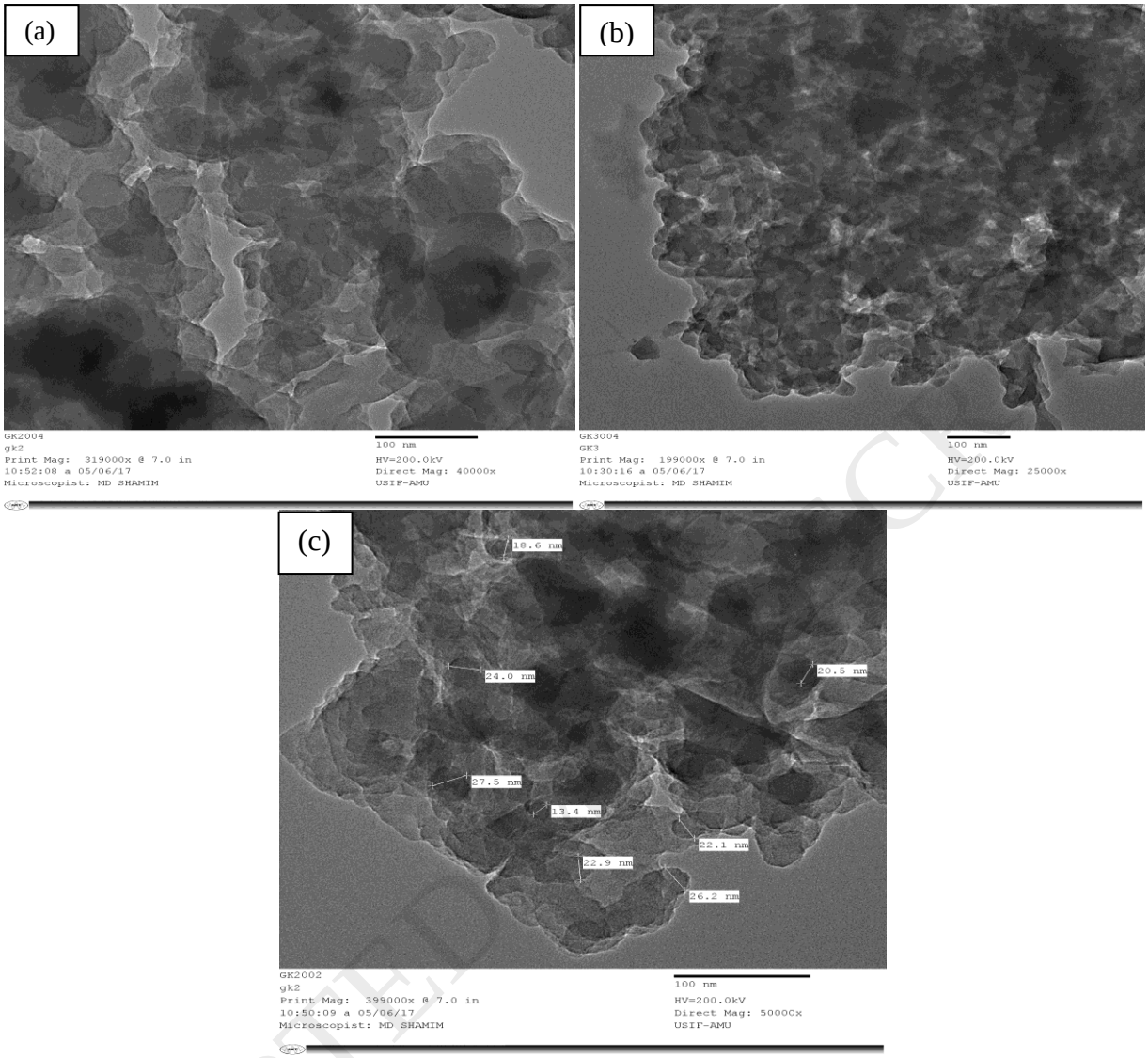

Fig. 6. TEM images of PANI/C/Ni bio-nanocomposite (a) and PANI/Ni nanocomposites (b, c).

ACCEPTED MANUSCRIPT

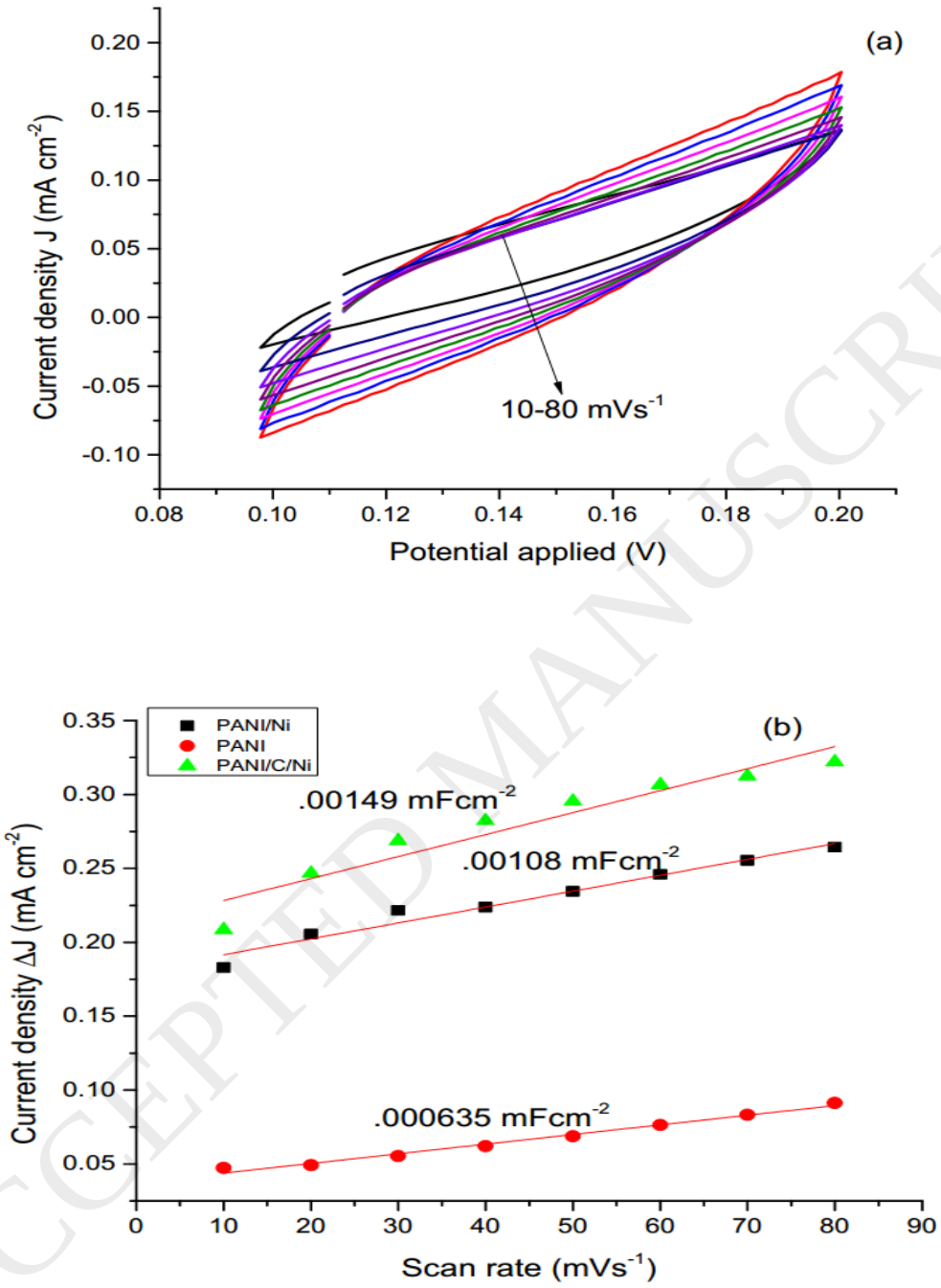

Fig. 7. (a) Cyclic Voltammograms of the as prepared bio-nanocomposites at different scan rate 10-80 mVs^{-1} and (b) ECSA of the PANI, PANI/Ni and PANI/C/Ni.

ACCEPTED MANUSCRIPT

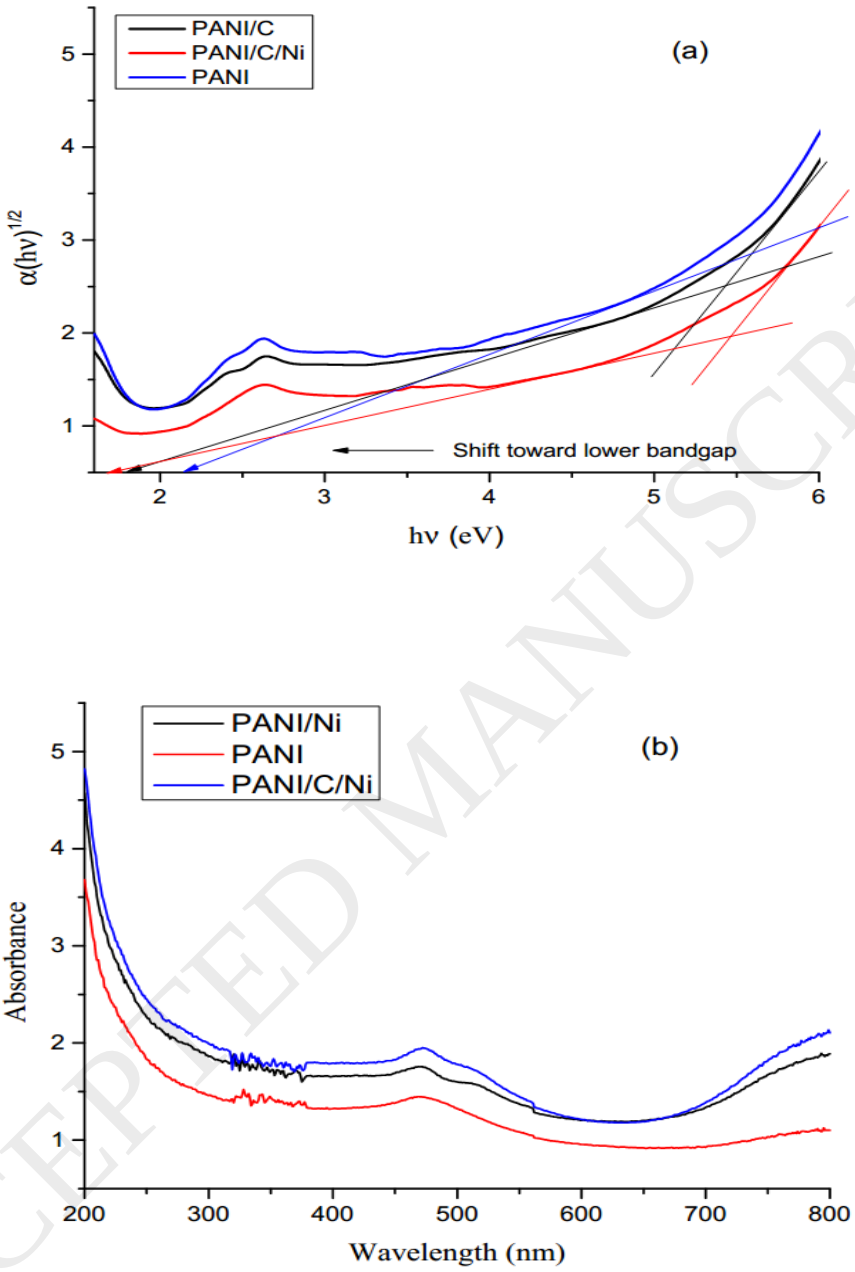

Fig. 8. (a)Tauc plots spectra for the band gap calculation of the as prepared materials and (b) UV-DRS absorption spectra of the materials.

ACCEPTED MANUSCRIPT

ACCEPTED MANUSCRIPT

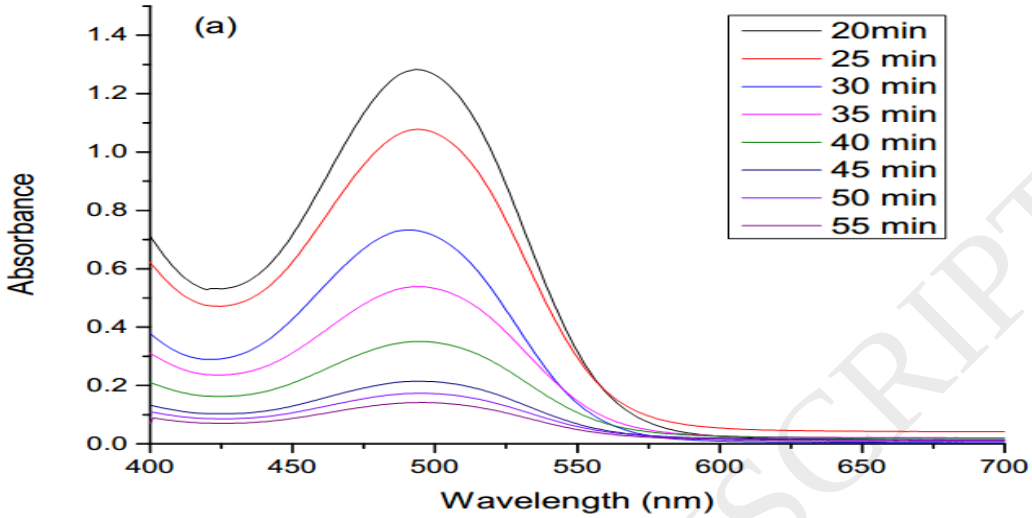

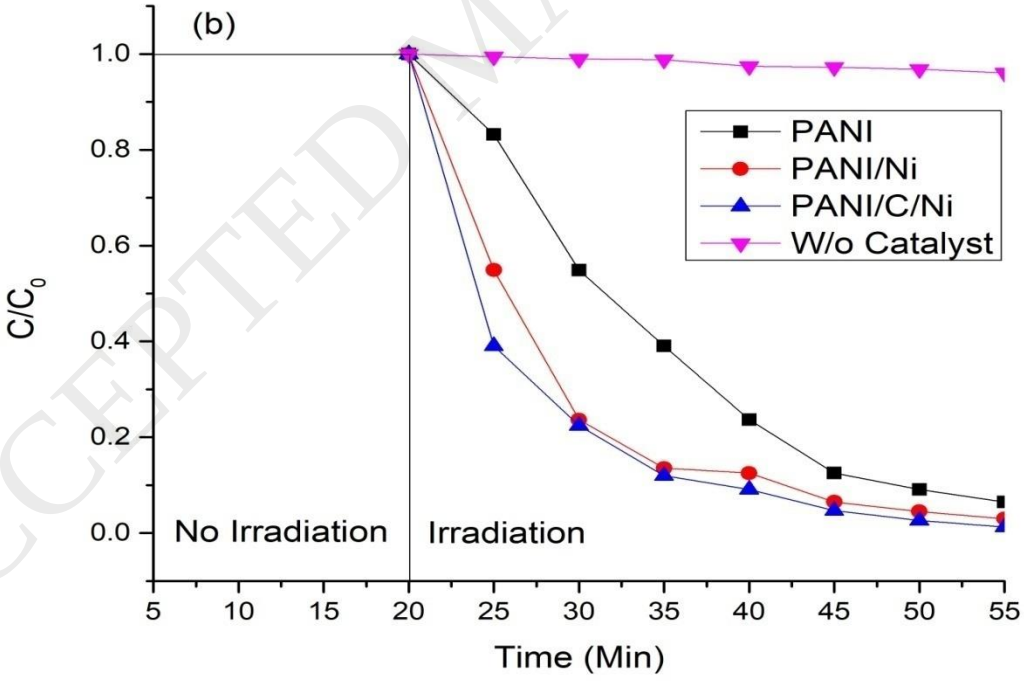

ACCEPTED MANUSCRIPT

ACCEPTED MANUSCRIPT

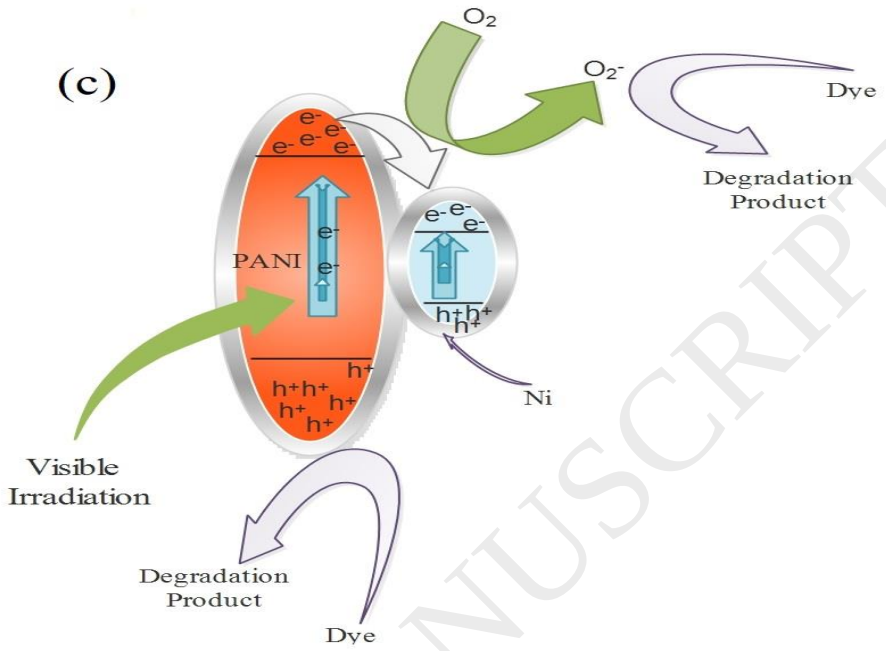

Fig.9. (a) Visible spectra of the as prepared materials (b) Kinetics of photodegradation and (c) Probable mechanism for the photodegradation of the RO-16 dye.

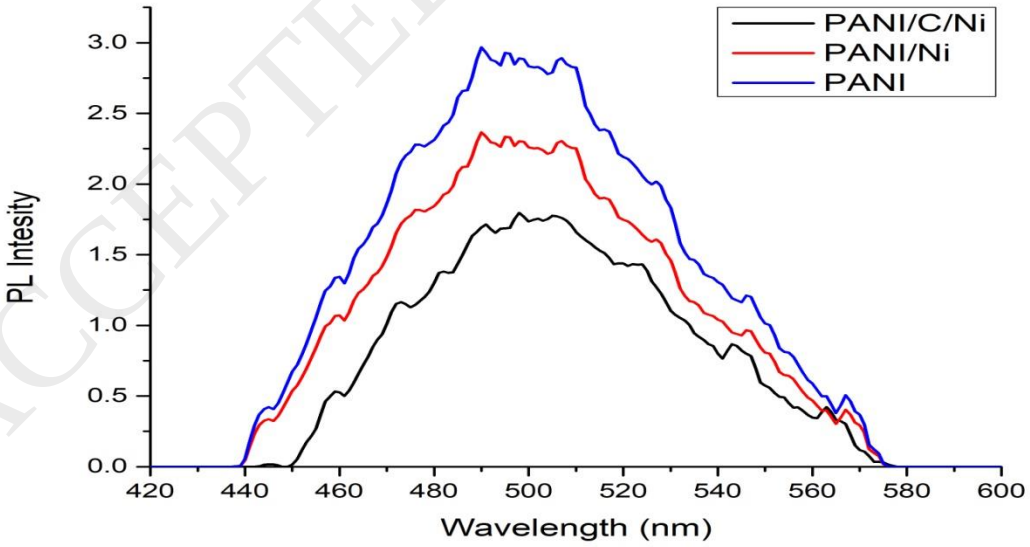

Fig.10. Photoluminescence spectra of the samples under investigation.

ACCEPTED MANUSCRIPT

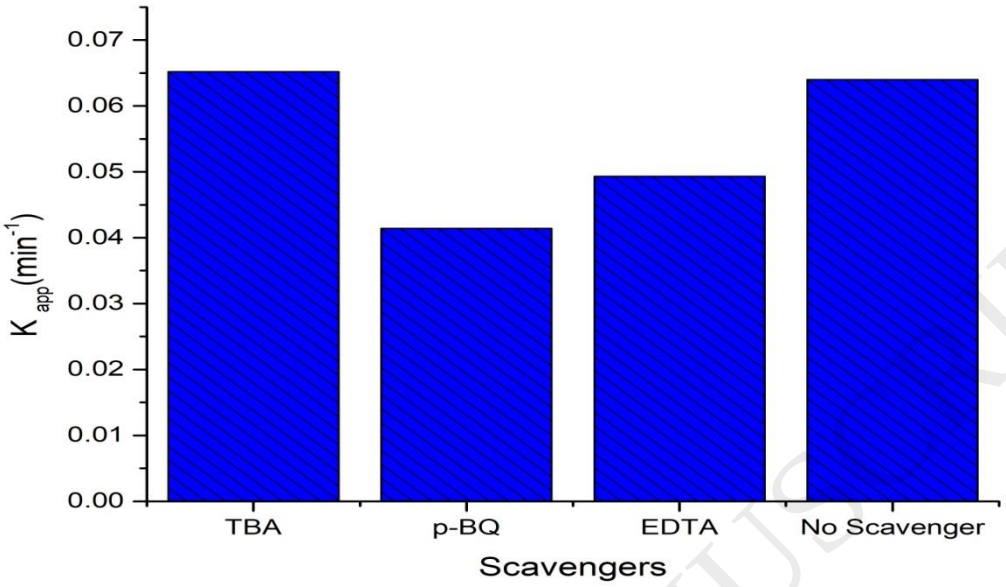

Fig.11. Effect of scavengers on the photodegradation of dye over bionanocomposite photocatalyst.

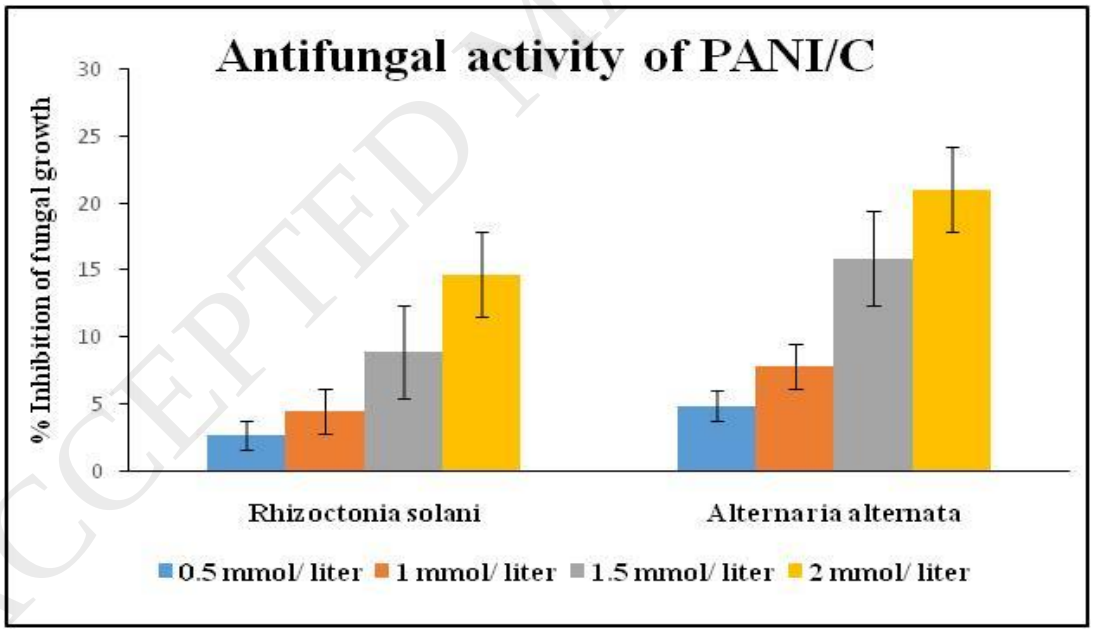

ACCEPTED MANUSCRIPT

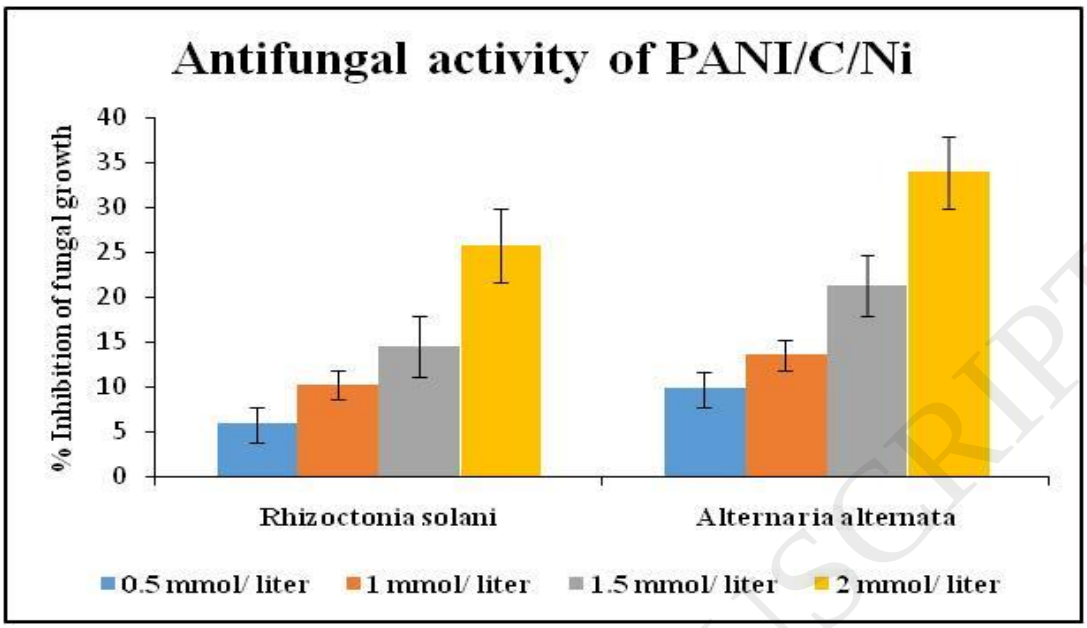

Fig.12. Per cent inhibition of fungal growth in presence of PANI/C and PANI/C/Ni.

ACCEPTED MANUSCRIPT

ACCEPTED MANUSCRIPT

Table. 1

S.No.	Polyaniline based nanocomposites	Type of dye	Percent degradation efficiency of dye	Irradiation Time (Min)	References
1	Polyaniline/ZnO nanocomposite	Malachite green (MG) and Methylene blue (MB)	79% of MB 89% of MG	300	[51]
2	Chitosan grafted-polyaniline/Co_3O_4	Methylene Blue	88%	180	[52]
3	Polyaniline/TiO_2	Reactive Red 45	98%	60	[53]
4	Polyaniline-nickel ferrite nano-composite	Methylene Blue	88.13%	120	[54]
5	Polyaniline/silver/silver phosphate	Rhodamine B	95%	5	[55]
6	Polyaniline/Zr-Co substituted nickel ferrite	Methylene Blue	97%	150	[56]
7	Polyaniline/cellulose/Ni	Reactive Orange -16	93%	55	Present study

Table. 1 A comparative study of polyaniline based nanocomposites for the photodegradation of different dyes.

ACCEPTED MANUSCRIPT

ACCEPTED MANUSCRIPT

Table. 2

A tabular representation of the properties of as prepared materials PANI, PANI/Ni and PANI/C/Ni in given in table. 2.

Materials	*hkl* values with 2θ values	Average crystallite size	Electrochemical surface area	Rate constant of photodegradation
PANI	2θ *hkl* 25.6º (2,0,0) 15.6º (0,1,1)	223 nm	.000635 $mFcm^{-2}$	.049 min^{-1}
PANI/Ni	2θ *hkl* 25.50º (2,0,0) 29.40º (0,0,2)	58 nm	.00108 $mFcm^{-2}$	.064 min^{-1}
PANI/C/Ni	2θ *hkl* 17.20º (0,0,1) 19.80º (1,0,0) 26.0º (2,0,0) 30.0º (0,0,2) 36.4º (1,1,0) 41.2º (1,1,1)	50 nm	.00149 $mFcm^{-2}$	.08 min^{-1}

ACCEPTED MANUSCRIPT